The Astrophysical Journal Letters, 952:L40 (8pp), 2023 August 1 https://doi.org/10.3847/2041-8213/acce9f

Statistical Study of Anisotropic Proton Heating in Interplanetary Magnetic Switchbacks Measured by Parker Solar Probe

Qiaowen Luo[1,2], Die Duan[2], Jiansen He[2], Xingyu Zhu[2], Daniel Verscharen[3], Jun Cui[1], and Hairong Lai[1]
[1] School of Atmospheric Sciences, Sun Yat-sen University, Zhuhai 519000, People's Republic of China; jshept@pku.edu.cn, cuijun7@mail.sysu.edu.cn
[2] School of Earth and Space Sciences, Peking University, Beijing 100871, People's Republic of China; laihr@mail.sysu.edu.cn
[3] Mullard Space Science Laboratory, University College London, Dorking RH5 6NT, UK
Received 2023 February 12; revised 2023 April 1; accepted 2023 April 3; published 2023 August 1

Abstract

Magnetic switchbacks, which are large angular deflections of the interplanetary magnetic field, are frequently observed by Parker Solar Probe (PSP) in the inner heliosphere. Magnetic switchbacks are believed to play an important role in the heating of the solar corona and the solar wind as well as the acceleration of the solar wind in the inner heliosphere. Here, we analyze magnetic field data and plasma data measured by PSP during its second and fourth encounters, and select 71 switchback events with reversals of the radial component of the magnetic field at times of unchanged electron-strahl pitch angles. We investigate the anisotropic thermal kinetic properties of plasma during switchbacks in a statistical study of the measured proton temperatures in the parallel and perpendicular directions as well as proton density and specific proton fluid entropy. We apply the "genetic algorithm" method to directly fit the measured velocity distribution functions in field-aligned coordinates using a two-component bi-Maxwellian distribution function. We find that the protons in most switchback events are hotter than the ambient plasma outside the switchbacks, with characteristics of parallel and perpendicular heating. Specifically, significant parallel and perpendicular temperature increases are seen for 45 and 62 of the 71 events, respectively. We find that the density of most switchback events decreases rather than increases, which indicates that proton heating inside the switchbacks is not caused by adiabatic compression, but is probably generated by nonadiabatic heating caused by field–particle interactions. Accordingly, the proton fluid entropy is greater inside the switchbacks than in the ambient solar wind.

Unified Astronomy Thesaurus concepts: Solar wind (1534); Alfven waves (23); Heliosphere (711)

Supporting material: animation

1. Introduction

An abundance of magnetic field deflections, which form a so-called "switchback" geometry, have been observed by Parker Solar Probe (PSP) during its encounters with the Sun (Bale et al. 2019; Kasper et al. 2019). Magnetic switchbacks often behave like large-amplitude Alfvénic disturbances, which are characterized by nearly constant field strength ($|B|$), a reversal of the radial magnetic field component (B_R), and an associated enhancement in the radial fluid velocity component (V_R) (McComas et al. 1998; Landi et al. 2006; Matteini et al. 2014, 2015). Magnetic switchbacks usually occur in patches/clusters spanning over time intervals ranging from hours to days and are separated by intervals of relatively quiet magnetic fields (Bale et al. 2019; Kasper et al. 2019; Horbury et al. 2020).

Generally, there are five classes of potential explanations for the origin of magnetic switchbacks. In the first scenario, interchange magnetic reconnection between open and closed field lines is invoked to generate the magnetic kinks, which propagate upward and nonlinearly develop in the inner heliosphere (Axford & McKenzie 1997; Fisk 2005; Zank et al. 2020; Magyar et al. 2021a, 2021b; He et al. 2021). In the second scenario, magnetic flux ropes with helical flows are launched from interchange magnetic reconnection sites and form the observed interplanetary magnetic switchbacks (Fisk & Kasper 2020; Bale et al. 2021; Drake et al. 2021; Zank et al. 2021). The third scenario evokes the shuffling motion of magnetic field line footpoints in the photosphere as a driver of Alfvénic fluctuations propagating upward, leaving some of them at shorter wavelength surviving through the stratified solar atmosphere to nonlinearly form magnetic switchbacks (Matteini et al. 2015; Squire et al. 2020; Tenerani et al. 2020; Jakab & Brandenburg 2021). The fourth scenario involves the local production of magnetic switchbacks by Kelvin–Helmholtz instability in flow velocity shear regions (Landi et al. 2006; Ruffolo et al. 2020). In the fifth scenario, magnetic switchbacks are segments of the super-Parker-spiral interplanetary magnetic field, the formation of which is caused by the change from slow solar wind to fast solar wind at different heliocentric distances within the same magnetic flux tube (Schwadron & McComas 2021).

Recent studies have focused on the nature and evolution of switchbacks using PSP observations and numerical simulations (Dudok de Wit et al. 2020; Farrell et al. 2020; Horbury et al. 2020; Krasnoselskikh et al. 2020; McManus et al. 2020; Mozer et al. 2020; Tenerani et al. 2020, 2021; Pecora et al. 2022; Shi et al. 2022). Switchbacks are actively embedded in the turbulent cascade by injecting additional energy into the background inertial range (Hernández et al. 2021). At switchback boundaries, evidence of magnetic reconnection (Froment et al. 2021) and small-scale wave activity (Mozer et al. 2020) has been observed that may dissipate the energy of the switchbacks. MHD simulations of a single switchback show

that the switchback can be eventually destroyed by a parametric decay process (Tenerani et al. 2020), thus transferring energy to the background plasma.

The properties of the plasma inside the switchback seem to be complicated and not well understood. Studies have shown that the proton temperature increases inside switchbacks (Farrell et al. 2020; Mozer et al. 2020; Liu et al. 2022), while Woolley et al. (2020) find that the proton core parallel temperature is similar inside and outside switchbacks. This latter finding is consistent with the interpretation that switchbacks are Alfvénic pulses traveling along open magnetic field lines. Verniero et al. (2020) present the first analysis of 3D proton velocity distribution functions (VDFs) inside and outside a switchback at 35 solar radii and find that the temperature remains largely unchanged through the field reversal. Using measurements from the PSP/SPAN-Ai instrument, Woodham et al. (2021) observe that inside the switchback patches in encounter 2, the parallel proton temperature is enhanced while the perpendicular proton temperature remains nearly constant. In order to further analyze the temperatures and the thermal anisotropy of protons inside and outside switchbacks, our work provides a statistical analysis combining the observational data from PSP and the fit results from the "genetic algorithm" (GA) method.

Entropy is an important thermodynamic property of the solar wind. For a simple magnetohydrodynamic (MHD) model with scalar pressure, the entropy is defined as $S = c_v \ln(P_{\rm p}/n_{\rm p}^{\gamma})$, where $P_{\rm p} = n_{\rm p} k_{\rm B} T_{\rm p}$ is the thermal pressure, $n_{\rm p}$ is the solar wind number density, $T_{\rm p}$ is the solar wind proton temperature, $k_{\rm B}$ is the Boltzmann constant, γ is a polytropic index, and c_v is a specific heat constant. There can be a positive or negative correlation between the solar wind proton temperature and the solar wind density, which affects the evolution of the solar wind entropy. Many studies have shown that the polytropic index usually ranges from 0.5 to 2.5, with 1.66 as the mean, equivalent to $5/3$ (Nicolaou et al. 2014; Livadiotis & Desai 2016; Livadiotis 2018). For a polytropic index of $\gamma = 5/3 (>1)$, entropy increases with distance, for example, due to the dissipation of turbulence, while entropy decreases if the polytropic index satisfies $\gamma < 1$ (Adhikari et al. 2020).

We perform a statistical analysis of the possible change of plasma parameters across magnetic switchbacks, including proton number density, proton temperature in the parallel and perpendicular directions, and specific entropy. We select 71 switchback events with reversals of the radial magnetic field component from its ambient background state during the second and fourth PSP encounters and analyze the above parameters separately. We have also analyzed the data from other encounters, and these observations of protons are similar to those of the second and fourth encounters. We apply the GA method (Holland 1992) to directly fit the measured VDFs in field-aligned coordinates using a 2D two-component bi-Maxwellian distribution function. This paper is organized as follows. In Section 2, we describe the PSP measurements and the GA method. Then we show the distributions of the fit parameters and compare them inside and outside the switchbacks. In Section 3, we discuss our results and draw our conclusions.

2. Observational Analysis and Model Comparison

The PSP mission operates at its highest sampling rates during the encounter phase when the spacecraft is at distances less than 0.25 au from the Sun (Fox et al. 2016). We use measurements from the encounter phase of the second and fourth orbits of PSP. The fluxgate magnetometer in the FIELDS instrument suite (Bale et al. 2016) provides the magnetic field $\boldsymbol{B}$, and the Solar Wind Electrons, Protons, and Alphas (SWEAP; Kasper et al. 2016) instrument suite provides the plasma data. This work utilizes the proton data measured by the Solar Probe Analyzer for ions on the ram-direction side of PSP (SPAN-Ai/SWEAP). We use the moments obtained from the VDF, including the proton number density ($n_{\rm p}$), the proton parallel and perpendicular temperatures ($T_{\parallel}$ and $T_{\perp}$), and the proton bulk velocity ($\boldsymbol{V}$).

We use the instant background magnetic field ($\boldsymbol{B}_0$) to define the magnetic field-aligned coordinates. The direction with the subscript "$\parallel$" is defined to be along $\boldsymbol{B}_0$. The direction with the subscript "$\perp 2$" denotes the vector product of the "$\parallel$"-direction and the vector pointing from the Earth to the Sun. The remaining third direction with the subscript "$\perp 1$" completes the right-hand system. For every PSP orbit, a significant portion of the solar wind plasma distribution is obscured by the spacecraft's heat shield and therefore lies outside SPAN's field of view (Kasper et al. 2016). Such partial occlusion leads to the truncation of proton VDFs in the "$\perp 1$"-dimension and significant inaccuracies in determining the plasma parameters through integration. Therefore, in the following analysis, we focus on the slice of the proton VDFs determined by the "$\parallel$"-direction and the unobscured perpendicular "$\perp 2$"-direction and their corresponding components of the proton bulk velocities and temperatures.

We select switchback events based on the criterion that the magnetic field radial component in the switchback intervals is opposite to their ambient background magnetic field radial component. During the second and fourth PSP perihelion encounters, the background magnetic field of the ambient intervals is sunward with $\theta_{\rm BR} > 160^{\circ}$ ($\theta_{\rm BR}$ is the angle between the radial direction and the magnetic field), and the magnetic field radial component of the switchbacks is antisunward with $B_{\rm R} > 0$. As a result, 71 switchback events are found during the two PSP encounters. Figure 1 shows an example of a switchback event, the interval of which is highlighted with a gray shaded area. The solar wind velocity components in RTN (radial–tangential–normal) coordinates ($V_{\rm R}$, $V_{\rm T}$, $V_{\rm N}$) in Figures 1(a)–(c), the proton number density $n_{\rm p}$ and the proton temperature $T_{\rm p}$ in Figure 1(d) are provided by measurements from SPAN-Ai. Compared to its ambient solar wind conditions, the density decreases while the temperature increases (see Figure 1(d)) inside the switchback. Figure 1(e) shows the specific proton fluid entropy per particle. We evaluate the specific proton fluid entropy as $S = (3/2)\ln(P_{\rm p}/n_{\rm p}^{5/3})$. The specific fluid entropy is enhanced inside the switchback, suggesting that plasma in the switchback has experienced a nonadiabatic heating process. Figure 1 (f) shows the time series of the magnetic pressure P_B (blue), the thermal pressure P_p (red), and the total pressure $P_B + P_p$ (black). During the whole time interval, the magnetic pressure is nearly constant while the thermal pressure decreases inside the switchback, resulting in a decrease in the total pressure.

Figure 2 presents our statistical results of the measured proton temperature in the parallel and perpendicular directions for both the switchback intervals and the ambient background intervals. In Figure 2, the parallel and perpendicular temperatures of the protons are estimated by the second-order moments

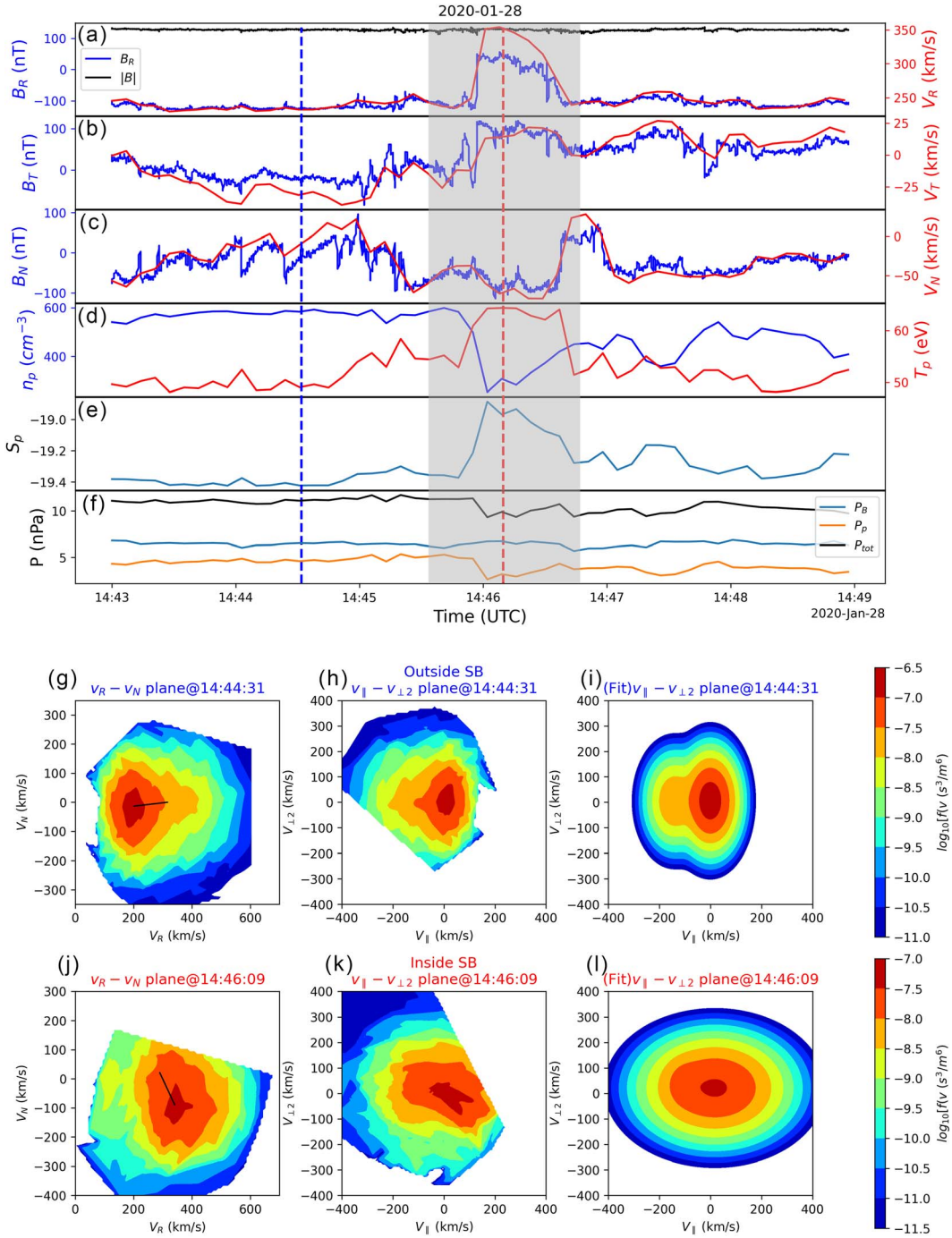

Figure 1. Example of a magnetic switchback event. (a)–(c) Time series of three components of the magnetic field (blue) and velocity (red) in RTN coordinates. The black line in panel (a) represents the magnetic field strength. (d) Time series of n_p (blue) and T_p (red). (e) Derived specific proton fluid entropy density. (f) Time sequences of magnetic pressure (blue), thermal pressure (red), and total pressure (black). The gray shaded area superposed on panels ((a)–(f)) denotes the switchback interval. The vertical dashed lines represent the times of the measured VDFs (blue: outside the switchback, red: inside the switchback). (g) Slice of the measured proton VDF outside the switchback in the V_R–V_N plane with V_T=0 at 14:44:31 on 2020 January 28. The black line indicates the direction of the local magnetic field. (h) Slice of the measured proton VDF in the $V_{//}$–$V_{\perp 2}$ plane with $V_{\perp 1} = 0$ at the same time as (g). (i) Fitted VDF of the observed 2D VDF, VDF($V_\parallel$, $V_{\perp 2}$) at the same time as (g). (j) Slice of the measured proton VDF inside the switchback in the V_R–V_N plane with V_T=0 at 14:46:09. (k) Slice of the measured proton VDF in the $V_{//}$–$V_{\perp 2}$ plane with $V_{\perp 1} = 0$ at the same time as (j). (l) Fitted VDF of the observed 2D VDF, VDF($V_\parallel$, $V_{\perp 2}$) at the same time as (j). A 3D animation of two dimension panels (g) and (j) is available. These two 3D velocity distribution functions show some rotation about the V_N axis before moving to a V_R rotation. The real-time duration of the video is 16 seconds.

(An animation of this figure is available.)

of the VDFs involving both the core and beam populations of protons without distinguishing them. We calculate the mean proton temperatures in the parallel and perpendicular directions of every switchback interval and every background/nonswitchback interval. We find increases in parallel temperature in 45 of the 71 switchback events (Figures 2(a)–(c)), and increases in perpendicular temperature in 62 of the 71 switchback events (Figures 2(d)–(f)). Figure 2(g) shows the

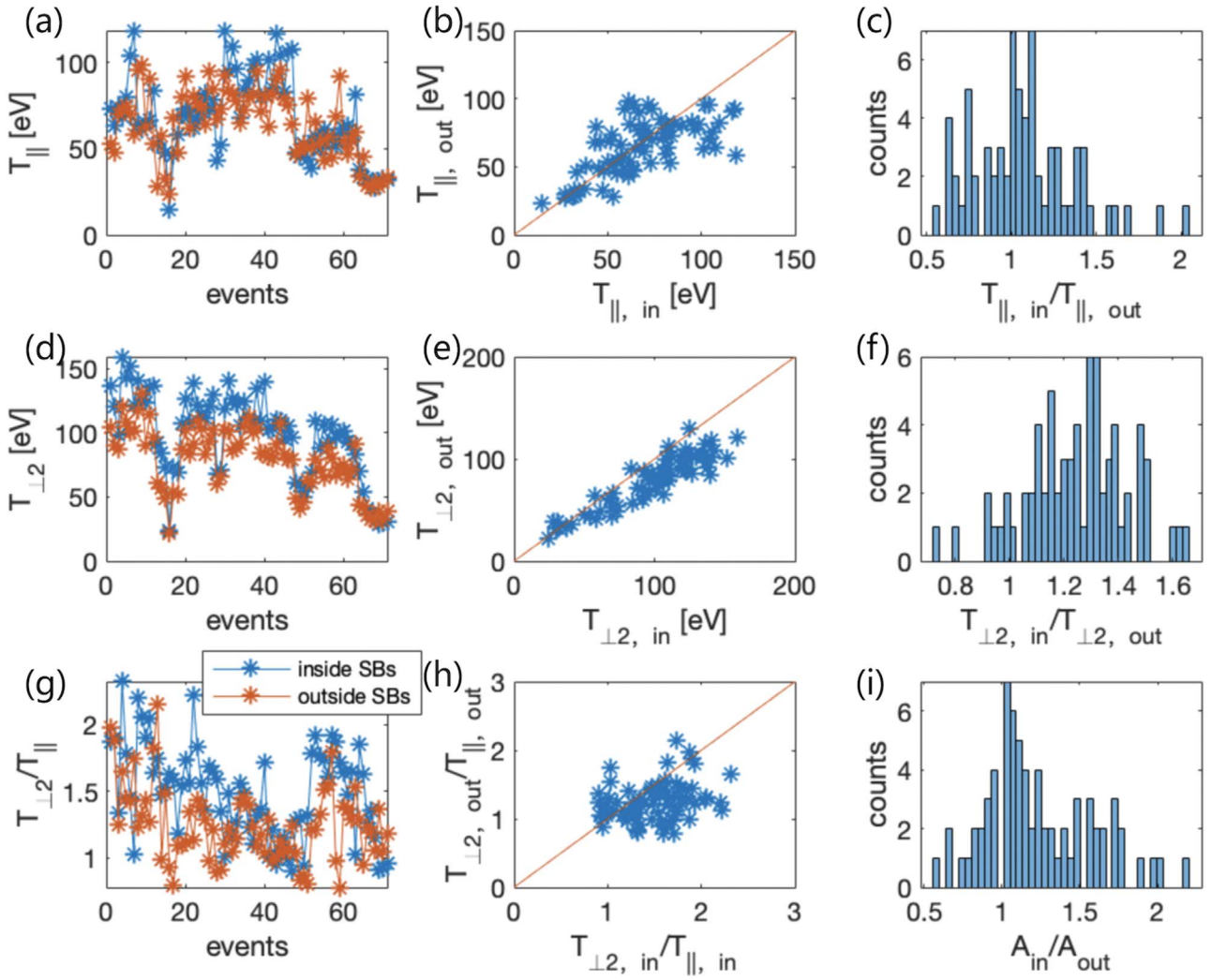

Figure 2. (a) and (d) Averaged temperatures of the switchback intervals (blue) and their ambient background intervals (red) in the parallel direction (see panel (a)) and the perpendicular direction (see panel (d)). (b) and (e) Statistical comparison of the parallel and perpendicular proton temperatures inside and outside the switchbacks.. (c) and (f) Statistical distribution histogram of the parallel temperature ratios inside and outside the switchbacks, and the perpendicular temperature ratios. (g) Thermal anisotropy ($T_{\perp 2}/T_{\parallel}$) of the switchback intervals (blue) and their ambient intervals (red). (h) Statistical comparison of the thermal anisotropy inside and outside the switchbacks. (i) Statistical histogram of the thermal anisotropy ratio, $A_{\rm in}/A_{\rm out}$, where $A = T_{\perp 2}/T_{\parallel}$.

proton thermal anisotropy $T_{\perp}/T_{\parallel}$, with switchback intervals in blue and ambient intervals in red. The proton temperature under investigation generally shows a thermal anisotropy, with $T_{\perp}/T_{\parallel} > 1$ in 64 of the 71 events of switchback intervals and in 61 of the 71 ambient intervals. The thermal anisotropy in the switchback events is even more prominent than outside the switchback intervals (see Figures 2(h) and 2(i)).

For all the switchback events analyzed, the ambient magnetic field is quasi-radial and the proton beam can move freely along the magnetic field as long as it does not drive any kinetic instabilities. Hence, the presence of a proton beam is often seen in the field of view (FOV) of SPAN-Ai since the beam component falls in the observable region of velocity space. As PSP moves deeper into a switchback, an increasing part of the velocity distribution may be observed as long as the solar wind flow is deflected toward the negative T direction in RTN coordinates. However, the observability can deteriorate when the solar wind flow inside the switchback is biased in the +T direction, in which case the beam population may be missed by falling out of the FOV of SPAN-Ai (Woodham et al. 2021). Therefore, the chance of detecting a beam inside a switchback is not as high as detecting it outside a switchback. For this reason, comparing the temperature changes of the proton core component inside and outside the switchback is an acceptable compromise to estimate the heating in switchbacks. We apply the GA method (Holland 1992) to directly fit the measured 2D cut of the VDFs in field-aligned coordinates, $f_{2D}(v_{\parallel}, v_{\perp})$, using a two-component bi-Maxwellian distribution function:

$$f_{2D}(v_{\parallel}, v_{\perp}) = \sum_{j=c,b} n_{\rm j}\left(\frac{1}{2\pi v_{{\rm th},\parallel,{\rm j}}^2}\right)^{1/2}\left(\frac{1}{2\pi v_{{\rm th},\perp,{\rm j}}^2}\right) \exp\left(-\frac{(v_{\parallel}-u_{\parallel,{\rm j}})^2}{2v_{{\rm th},\parallel,{\rm j}}^2}\right)\exp\left(-\frac{(v_{\perp}-u_{\perp,{\rm j}})^2}{2v_{{\rm th},\perp,{\rm j}}^2}\right) \quad (1)$$

where $j = c, b$ denotes the proton core and beam populations, respectively. There are 10 parameters to be fitted in Equation (1): the number densities ($n_{\rm j}$), the bulk velocity components in the two directions ($u_{\parallel,\,j}$ and $u_{\perp,\,j}$), and the thermal velocities ($v_{{\rm th}\parallel,\,j}$ and $v_{{\rm th}\perp,\,j}$) of the core and beam

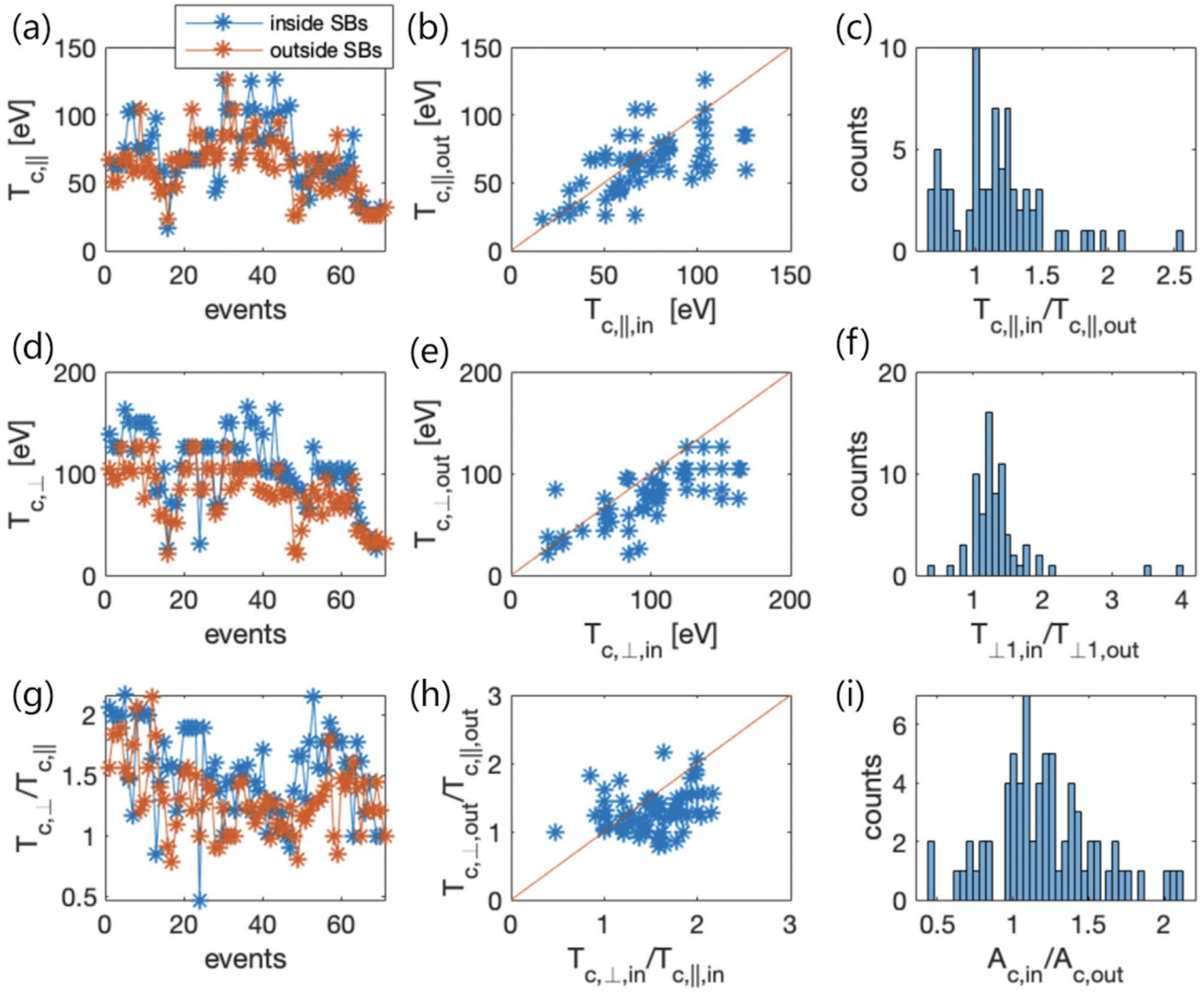

Figure 3. Proton core temperatures in the parallel and perpendicular directions as obtained from the GA fitting method. (a) and (d) Averaged Proton core temperatures in the parallel and perpendicular directions for the switchback intervals (blue) and the background intervals (red). (b) and (e) Statistical comparison of the parallel and perpendicular proton core temperatures inside and outside the switchback intervals. (c) and (f) Statistical histogram of the parallel temperature ratios inside and outside the switchbacks, and the perpendicular temperature ratios. (g) Proton core thermal anisotropy ($T_{c,\perp 2}/T_{c,\parallel}$) of the switchback intervals (blue) and their ambient intervals (red). (h) Statistical comparison of the proton core thermal anisotropy inside and outside the switchbacks. (i) Statistical histogram of the proton core thermal anisotropy ratio, $A_{c,in}/A_{c,out}$, where $A = T_{c,\perp 2}/T_{c,\parallel}$.

populations. The subscript "⊥" used here refers to the perpendicular component in the direction that is not significantly affected by the obscuration of the heat shield.

Figures 1(g)–(l) show examples of the measured and fitted VDFs outside a switchback at 14:44:31 and inside a switchback at 14:46:23 2020 January 28. We also show the 3D VDFs at both times in the Supplementary Materials.

The ability of the SPAN-i instrument to observe the proton beam depends on the direction of the magnetic field deflection associated with the switchback. If the magnetic field of the switchback deviates from the -R direction towards the -T direction, the beam cannot fall within the field of view (FOV) of SPAN-Ai, resulting in a lack of beam information in the measured velocity distribution function. For the sake of statistical consistency, we therefore only focus on the statistical analysis of the core component within the switchback.

Figure 3 displays the proton core temperatures in the parallel and perpendicular directions as obtained from the GA fitting method. We find enhancement of the proton core parallel temperature in 57 of the 71 switchback events and enhancement of the proton core perpendicular temperature in 66 of the 71 switchback events. Proton beams contribute to the estimated parallel proton temperatures outside the switchbacks in Figure 2, while the beam can hardly be observed inside the switchback. We find more events with enhanced parallel core temperature in the fitted results (see Figure 3(c)) than in the results from the moment integration of the parallel temperature (see Figure 2(c)). The proton core temperature shows a thermal anisotropy with $T_{\perp,c}/T_{\|,c} > 1$ in 65 of the 71 switchback events and 58 of the 71 measurements in the ambient plasma (Figures 3(g) and (h)). The thermal anisotropy is more pronounced inside than outside the switchbacks (Figure 3(i)).

Figure 4 shows our statistical results for $n_{p,}$ T_p, and S of the switchback intervals and the ambient intervals. n_p decreases in 67 of the 71 switchback events (Figures 4(a)–(c)) and T_p increases in 63 of the 71 switchback events (Figures 4(d)–(f)). As shown in Figure 4(g), S is not constant across the switchback boundaries, suggesting that the heating in these

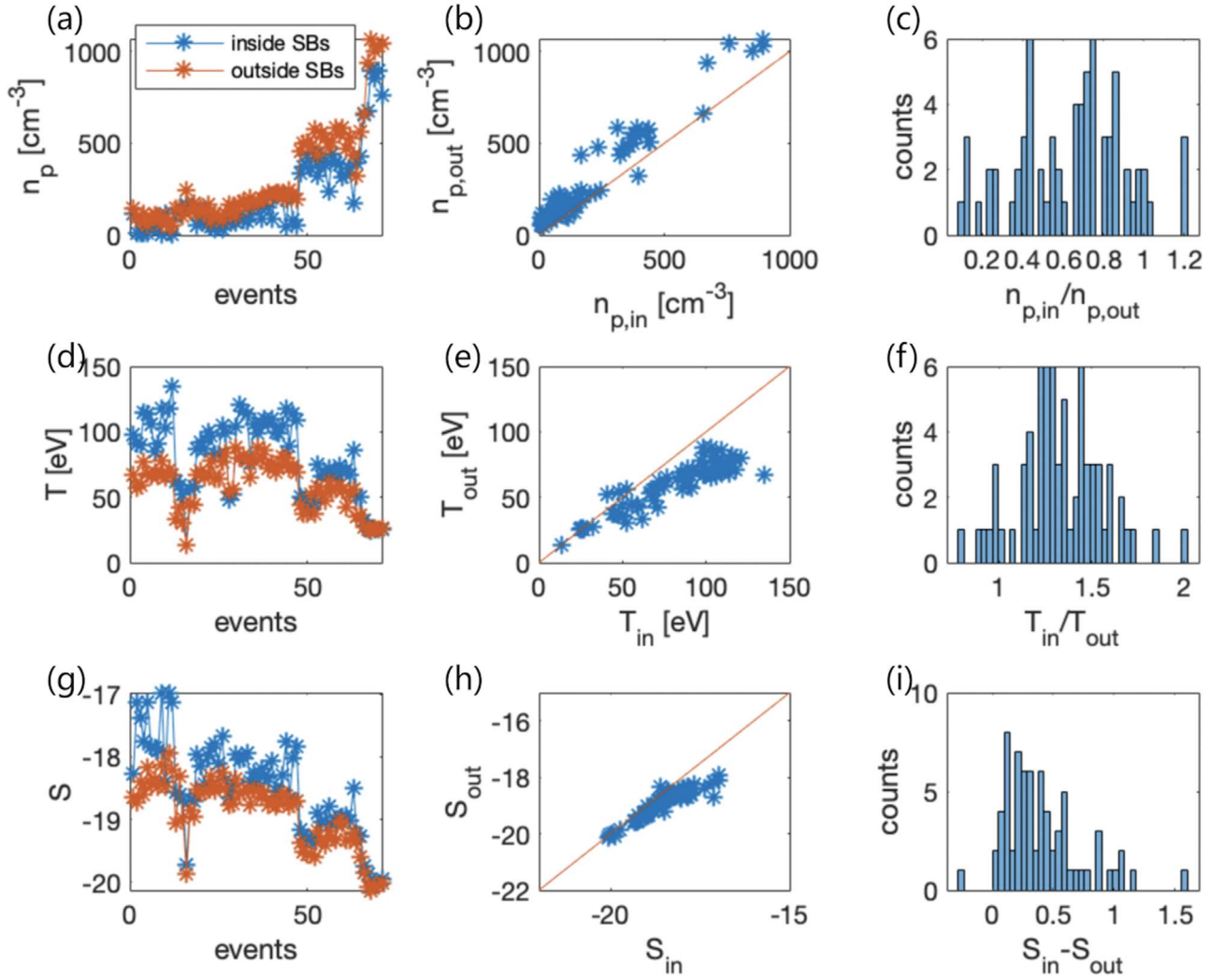

Figure 4. (a), (d) and (g) Averaged n_p, T_p, and S of the switchback intervals (blue) and their ambient intervals (red). (b), (e) and (h) Statistical comparison of n_p, T_p, and S inside and outside the switchbacks. (c), (f) and (i) Statistical histograms of n_p, T_p, and S inside and outside the switchbacks.

switchbacks is nonadiabatic. Moreover, S is greater than in the ambient intervals for 70 of the 71 switchback events.

If the switchback magnetic field rotates to the +N direction, a proton beams moves further into the FOV of SPAN-Ai. Figure 5 shows the VDFs in the SPAN-Ai instrument frame in the plane with $V_{\perp 1} = 0$ km s^{-1} at 15:48:29 on 2020 Jan 28 (outside switchback) and at 15:50:00 on 2020 Jan 28 (inside switchback). Outside the switchback, the proton beam is well observed flowing antiparallel to the magnetic field. As PSP moves deeper inside the switchback, the field-aligned proton beam remains visible. The 1D cuts of the fit results in Figures 5(c1) and (c2) also illustrate that, outside the switchback, the beam in the antiparallel direction well extends beyond the core, while inside the switchback, the beam in the antiparallel direction more strongly overlaps with the core of the VDF.

3. Summary and Discussion

Using PSP measurements of protons and magnetic fields in the inner heliosphere, we perform a statistical analysis of the proton number density, the proton parallel and perpendicular temperatures, and the specific proton fluid entropy in switchback events. We compare these quantities with those outside the switchbacks and in the ambient background solar wind to further investigate the plasma evolution during the switchback transition. We identify enhancements of the parallel proton temperature in 45 of the 71 switchback events, and enhancements of the perpendicular proton temperature in 62 of the 71 switchback events. We further find that the proton number density decreases in 67 of the 71 switchback events, and the specific proton fluid entropy increases in 70 of the 71 switchback events. According to the model by Tenerani et al. (2023), the heating of protons is due to compressions and phase space mixing. In our work, the decrease of density and increase of the proton fluid entropy indicates that proton heating inside the switchbacks may not be caused by adiabatic compression, but is probably generated by field–particle interactions. In our statistical analysis, we do not find clear observational evidence for phase space mixing, and it is worth to be further studied in future observation and simulation work. We find significant parallel and perpendicular temperature increases in 45 and 62 of the 71 events, respectively. The discovery of both parallel and perpendicular heating effects imposes observational constraints and sets a comparison goal for advancing the kinetic simulation of Alfvenic kinks. A recent simulation study

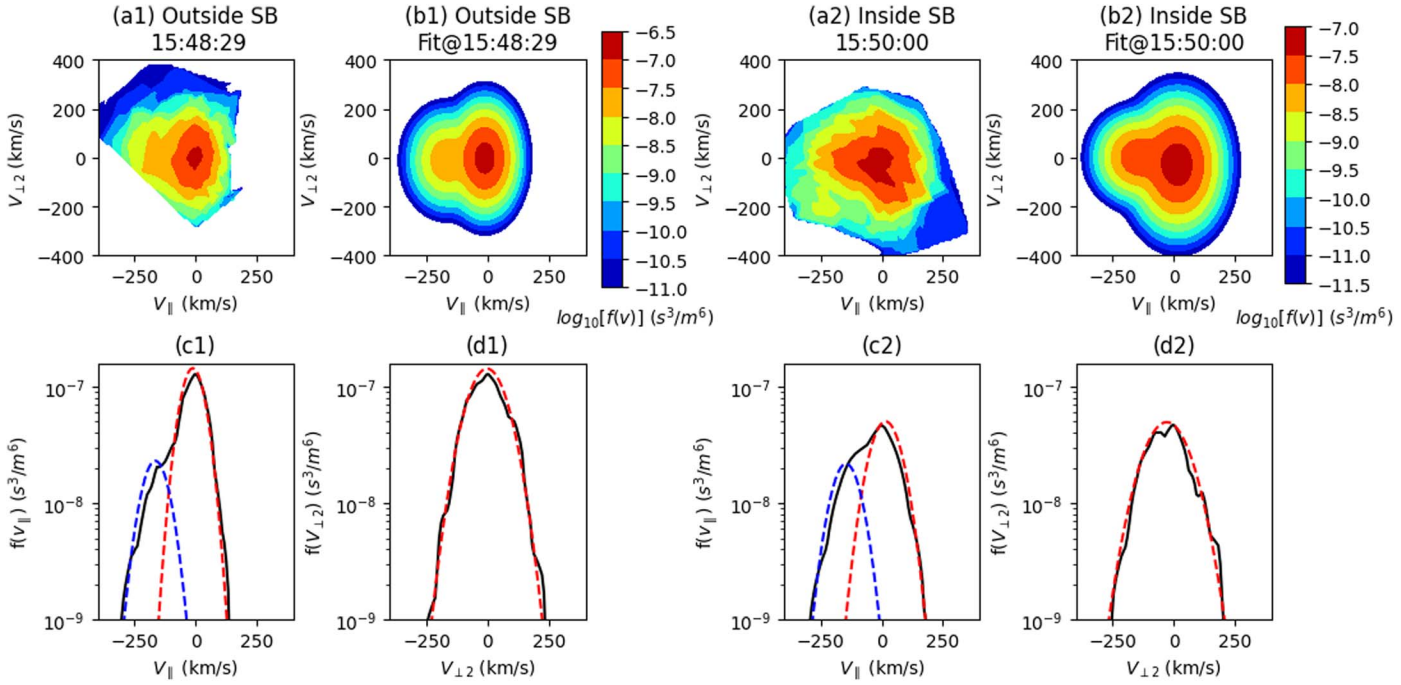

Figure 5. Example of a switchback event with proton beam appearing in the VDF. (a1) 2D slice of the measured proton VDF in the $V_{\perp 1} = 0$ km s^{-1} plane at 15:48:29 on 2020 Jan 28 (outside switchback). (b1) 2D fit result of the VDF in (a1) from the GA method. (c1) 1D cut of the measured 2D proton VDF in panel (a1) and fitted 2D proton VDF in panel (b1) along $V_\parallel$ and passing through the maximum value of the 2D VDF. The black line denotes the 1D cut of the measured VDF, while the green dotted line represents the 1D cut of the fitted VDF, with contributions from the proton core (red dotted line) and proton beam (blue dotted line). (d1) Same as panel (c1) but along $V_{\perp 2}$ rather than $V_\parallel$. (a2)–(d2) Same as (a1)–(d1) but at 15:50:00 on 2020 Jan 28 inside the switchback.

by Tenerani et al. (2023) models the proton parallel heating resulting from plasma compression and field-aligned phase space mixing.

Inside the switchbacks where the magnetic field vector deviates strongly from the radial direction, the quasi-field-aligned beam usually leaves the FOV of the SPAN-Ai instrument, complicating the analysis of proton thermodynamics. This means that the proton temperature, especially the parallel temperature, as obtained from the moment integration, is often not accurate. To address this issue, we apply the GA method to directly fit the measured VDFs in field-aligned coordinates using a 2D two-component bi-Maxwellian distribution function assuming gyrotropy. The thermal state of the core component can be estimated reliably without being affected by the lack of a complete beam measurement. This technique allows us to compare the temperature changes of the proton core inside and outside the switchback, which can reflect the heating to a certain extent. Due to the FOV limitations of SPAN-Ai, the kinetic effects of the proton beam in switchbacks cannot be well studied. Although we find that the beam characteristics outside of switchbacks are more prominent than inside, the role of proton beams inside switchbacks cannot be ignored. Proton beams can trigger instabilities (Liu et al. 2021) and are closely related to small-amplitude kinetic Alfvénic turbulence in the solar wind (He et al. 2015). The understanding of the differences in proton beam properties inside and outside of switchbacks and of the role of proton beams for the evolution of the switchbacks need further observations and simulations.

We identify enhancements of the proton core parallel and perpendicular temperatures in 57 and 66 of the 71 switchback events, respectively. Therefore, our combined analysis of the proton thermodynamics from PSP observations based on the moment method and the GA method suggests that the proton temperatures increase inside switchbacks in both the parallel and perpendicular direction in general. The heating of protons in switchbacks suggested by this study poses an observational constraint on future kinetic modeling of the interaction between switchback pulses and solar wind protons.

Acknowledgments

We acknowledge the NASA Parker Solar Probe mission team and the SWEAP team led by J. C. Kasper, and the FIELDS team led by S. D. Bale, for the use of PSP data. The data used in this paper can be downloaded from spdf.gsfc.nasa.gov. The work at Peking University is supported by NSFC (42241118, 42174194, 42150105, and 42204166), by National Key R&D Program of China (2021YFA0718600 and 2022YFF0503800), and by CNSA (D050106). D.D. is also funded by China Postdoctoral Science Foundation (2022M720213). The work at Sun Yat-sen University is supported by NSFC (2030201 and 42074209). D.V. from UCL is supported by STFC Consolidated Grants ST/S000240/1 and ST/W001004/1, and Ernest Rutherford Fellowship ST/P003826/1. We consider Qiaowen Luo and Die Duan due to their equal contributions to this work as co-first authors.

ORCID iDs

Qiaowen Luo https://orcid.org/0000-0001-7697-1186
Die Duan https://orcid.org/0000-0002-6300-6800
Jiansen He https://orcid.org/0000-0001-8179-417X
Xingyu Zhu https://orcid.org/0000-0002-1541-6397
Daniel Verscharen https://orcid.org/0000-0002-0497-1096
Jun Cui https://orcid.org/0000-0002-4721-8184
Hairong Lai https://orcid.org/0000-0001-5750-7919

References

Adhikari, L., Zank, G. P., Zhao, L. L., & Webb, G. M. 2020, ApJ, 891, 34
Axford, W. I., & McKenzie, J. F. 1997, in Cosmic Winds and the Heliosphere, ed. J. R. Jokipii, C. P. Sonett, & M. S. Giampapa (Tucson, AZ: Univ. of Arizona), 31
Bale, S. D., Badman, S. T., Bonnell, J. W., et al. 2019, Natur, 576, 237
Bale, S. D., Goetz, K., Harvey, P. R., et al. 2016, SSRv, 204, 49
Bale, S. D., Horbury, T. S., Velli, M., et al. 2021, ApJ, 923, 174
Drake, J. F., Agapitov, O., Swisdak, M., et al. 2021, A&A, 650, A2
Dudok de Wit, T., Krasnoselskikh, V. V., Bale, S. D., et al. 2020, ApJS, 246, 39
Farrell, W. M., MacDowall, R. J., Gruesbeck, J. R., Bale, S. D., & Kasper, J. C. 2020, ApJS, 249, 28
Fisk, L. A. 2005, ApJ, 626, 563
Fisk, L. A., & Kasper, J. C. 2020, ApJL, 894, L4
Fox, N. J., Velli, M. C., Bale, S. D., et al. 2016, SSRv, 204, 7
Froment, C., Krasnoselskikh, V., Dudok de Wit, T., et al. 2021, A&A, 650, A5
He, Jiansen, Wang, Linghua, Tu, Chuanyi, Marsch, Eckart, & Zong, Qiugang 2015, ApJL, 800, L31
He, J., Zhu, X., Yang, L., et al. 2021, ApJL, 913, 8
Hernández, C. S., Sorriso-Valvo, L., Bandyopadhyay, R., et al. 2021, ApJL, 922, L11
Holland, J. H. 1992, Adaptation in Natural and Artificial Systems: An Introductory Analysis with Applications to Biology, Control, and Artificial Intelligence (Cambridge, MA: MIT Press)
Horbury, T. S., Woolley, T., Laker, R., et al. 2020, ApJS, 246, 45
Jakab, P., & Brandenburg, A. 2021, A&A, 647, A18
Kasper, J. C., Abiad, R., Austin, G., et al. 2016, SSRv, 204, 131
Kasper, J. C., Bale, S. D., Belcher, J. W., et al. 2019, Natur, 576, 228
Krasnoselskikh, V., Larosa, A., Agapitov, O., et al. 2020, ApJ, 893, 93
Landi, S., Hellinger, P., & Velli, M. 2006, GeoRL, 33, L14101
Liu, R., Liu, Y. C. M., Huang, J., et al. 2022, JGRA, 127, e30382
Liu, Wen, Zhao, Jinsong, Xie, Huasheng, et al. 2021, ApJ, 920, 158
Livadiotis, G. 2018, Entrp, 20, 799
Livadiotis, G., & Desai, M. I. 2016, ApJ, 829, 88
Magyar, N., Utz, D., Erdélyi, R., & Nakariakov, V. M. 2021a, ApJ, 911, 75
Magyar, N., Utz, D., Erdélyi, R., & Nakariakov, V. M. 2021b, ApJ, 914, 8
Matteini, L., Horbury, T. S., Neugebauer, M., & Goldstein, B. E. 2014, GeoRL, 41, 259
Matteini, L., Horbury, T. S., Pantellini, F., Velli, M., & Schwartz, S. J. 2015, ApJ, 802, 11
McComas, D. J., Bame, S. J., Barraclough, B. L., et al. 1998, GeoRL, 25, 1
McManus, M. D., Bowen, T. A., Mallet, A., et al. 2020, ApJS, 246, 67
Mozer, F. S., Agapitov, O. V., Bale, S. D., et al. 2020, ApJS, 246, 68
Nicolaou, G., Livadiotis, G., & Moussas, X. 2014, SoPh, 289, 1371
Pecora, F., Matthaeus, W. H., Primavera, L., et al. 2022, ApJL, 929, L10
Ruffolo, D., Matthaeus, W. H., Chhiber, R., et al. 2020, ApJ, 902, 94
Schwadron, N. A., & McComas, D. J. 2021, ApJ, 909, 95
Shi, C., Panasenco, O., Velli, M., et al. 2022, ApJ, 934, 152
Squire, J., Chandran, B. D. G., & Meyrand, R. 2020, ApJL, 891, L2
Tenerani, A., González, C., Sioulas, N., Shi, C., & Velli, M. 2023, arXiv:2302.06150
Tenerani, A., Sioulas, N., Matteini, L., et al. 2021, ApJL, 919, L31
Tenerani, A., Velli, M., Matteini, L., et al. 2020, ApJS, 246, 32
Verniero, J. L., Larson, D. E., Livi, R., et al. 2020, ApJS, 248, 5
Woodham, L. D., Horbury, T. S., Matteini, L., et al. 2021, A&A, 650, L1
Woolley, T., Matteini, L., Horbury, T. S., et al. 2020, MNRAS, 498, 5524
Zank, G. P., Nakanotani, M., Zhao, L. L., Adhikari, L., & Kasper, J. 2020, ApJ, 903, 1
Zank, G. P., Zhao, L. L., Adhikari, L., et al. 2021, PhPl, 28, 080501